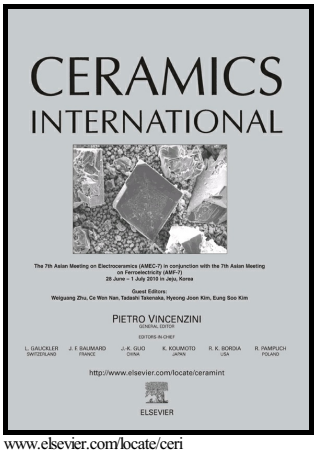

www.elsevier.com/locate/ceri

Solution processing of TiO_2 compact layers for 3rd generation photovoltaics

Cecile Charbonneau, Petra J. Cameron, Adam Pockett, Anthony Lewis, Joel Troughton, Eifion Jewell, David Worsley, Trystan Watson

PII: S0272-8842(16)30533-8
DOI: http://dx.doi.org/10.1016/j.ceramint.2016.04.125
Reference: CERI12743

To appear in: *Ceramics International*

Received date: 22 January 2016
Revised date: 31 March 2016
Accepted date: 22 April 2016

Cite this article as: Cecile Charbonneau, Petra J. Cameron, Adam Pockett Anthony Lewis, Joel Troughton, Eifion Jewell, David Worsley and Trystar Watson, Solution processing of TiO_2 compact layers for 3rd generatio photovoltaics, *Ceramics International* http://dx.doi.org/10.1016/j.ceramint.2016.04.125

Solution processing of TiO_2 compact layers for 3rd generation photovoltaics

Cecile Charbonneau[a,*], Petra J. Cameron[b], Adam Pockett[b], Anthony Lewis[a], Joel Troughton[a], Eifion Jewell[a], David Worsley[a] and Trystan Watson[a]

[a]SPECIFIC – College of Engineering, Swansea University, Baglan Bay Innovation & Knowledge Centre, Central Avenue, Baglan, Port Talbot, SA12 7AX

[b]University of Bath – Department of Chemistry, 1 South 1.20, Bath, BA27AY

*Corresponding author: c.m.e.charbonneau@swansea.ac.uk

Abstract

In this study, we introduce a new method for the deposition of TiO_2 compact layers which involves the deposition of a wet film of an inorganic titanium (IV) precursor followed by fast hydrolytic conversion to crystalline TiO_2 under near infrared radiative (NIR) treatment. With this, we aim to provide a scalable alternative to methods conventionally employed in laboratories for the fabrication of 3rd generation photovoltaic devices, such as high temperature pyrolysis or spin coating of organic titanium (IV) precursors. Optimization of our solution process is presented in detail. Structural features and crystalline properties of solution processed compact layers are characterized by FEG-SEM imaging and x-ray diffraction analyses and compared to compact layers produced by conventional laboratory techniques. Minimization of electron recombination is evaluated in standard liquid I^-/I_3^- dye-sensitized solar cells (DSC). The results show that a compact, homogenous, high coverage yield crystalline TiO_2 anatase layer can be produced by sequential deposition of 2 to 3 solution processed titanium oxide layers, each in under 30s. In standard liquid I^-/I_3^- DSC the solution processed compact layers strongly increased the electron lifetime, τ_n, when compared to cells prepared on a bare FTO substrate.

Keywords

TiO_2 compact layer; solution processing; near-infrared sintering; 3rd generation photovoltaics

Introduction

The fabrication of dye-sensitized solar cells (DSC) and more recent technologies such as lead-halide perovskite solar cells usually involves the deposition of a very thin (50-150 nm) and compact layer of TiO_2 at the surface of the photo-electrode substrate. This layer ensures the transfer of electrons photo-generated by the dye-sensitized mesoporous oxide or lead-halide perovskite layer to the transparent conductive oxide (TCO) of the substrate while minimizing the occurrence of short-circuits generated by electron recombination, a phenomenon also referred to as shunting [1-15]. In I^-/I_3^- based liquid dye-sensitized solar cells, the recombination of electrons at the substrate is a relatively slow process, hence the application of a TiO_2 blocking layer is known to moderately improve device performance. However, the presence of this layer is critical to the performance of liquid devices using the Co(III)/Co(II) electrolyte systems [16] and solid-state DSCs [2-5]. In these systems the electron recombination occurring at the interface between the TCO/hole transporter is approximately two orders of magnitude faster than in I^-/I_3^- liquid-based DSCs, hence the blocking layer plays a critical role in the fabrication of functional devices. In the case of lead-halide perovskite solar cells, the TiO_2 blocking layer acts as an n-type contact and minimizes electron back transfers from the FTO surface which allows the fabrication of high voltage devices. A number of titania

deposition methods have been suggested such as spin coating, atomic layer deposition, sputtering, etc. [12-15]. A few research groups have reported on the fabrication of blocking layer-free lead-halide perovskite solar cells [17], however the majority of high performance devices contain an inorganic or organic electron collection layer.

The TiO_2 blocking layer is usually produced with a thickness in the range 50-150 nm, depending on the type of 3rd generation PV technology and on the fabrication method. The thickness is ultimately optimized to minimize resistive losses [4,15] while ensuring enough material has been deposited to provide a high coverage yield over the substrate. The TiO_2 bocking layer is conventionally deposited using a multi-cycle spray pyrolysis technique [1,2,4,18]. A liquid organic titanium precursor, such as titanium diisopropoxide bis(acetylacetonate) (TAA), is sprayed over the conductive side of a TCO-glass substrate maintained at high temperature (up to 450 °C) on a hotplate. The build-up of a 50-150 nm compact layer requires the application of a large number of spray cycles, each of them separated by time intervals of approximately 10s allowing solvent evaporation and crystallization of the TiO_2. Although widely employed in laboratories, this method presents a number of technical difficulties, in particular low reproducibility associated to the manual aspect of the operation, and safety hazards associated to the spraying of flammable solvents over high temperature surfaces. Finally, the multi-step time consuming nature of the operation makes it particularly unsuited to large scale manufacturing of DSC or perovskite devices. Other methods are currently under development such as spin coating [19,20] which have been designed for the fast deposition of thicker TiO_2 compact layers, up to 225 nm [15]. Here again, this laboratory technique is relatively well suited and reproducible for substrates of small dimensions < 2 x 2 cm^2, but cannot be transferred to roll-to-roll manufacturing and presents real technical challenges when applied to larger substrates. Another more recent approach consists of using atomic layer deposition (ALD) of very thin TiO_2 layers, especially in the case halide perovskite devices where 2 nm of material is sufficient to prevent electron recombination effectively [13]. However, this technology is associated to high production costs due to the very slow deposition rates of material and vacuum nature of the process.

In order to address the large-scale process bottlenecks associated with conventional deposition of TiO_2 compact layers, a new method was developed in our laboratories: a solution of titanium (IV) chloride tetrahydrofurane ($TiCl_4$·THF) prepared in a mixed water/isopropanol solvent was coated, dried and hydrolyzed into a thin layer of crystalline TiO_2; the conversion of the precursor was induced by a fast heating of the FTO-glass substrate in under 0.5 minute using near infrared (NIR) radiation under atmospheric pressure conditions [21]. The application of NIR radiation has already proven successful for a number of applications, namely i) for the sintering of TiO_2 mesoporous films [22], ii) the platinization of TCO-glass counter electrodes [23] and iii) the curing of silver inks [24]. The main advantage of this NIR radiative method relates to the very short, roll-to-roll compatible processing time (< 30s) required for the full conversion of the precursor solution into crystalline TiO_2 compared to the 30 mins oven/hotplate sintering step conventionally used in laboratories. This is largely facilitated because of the chemical nature of the precursor: unlike organo-Ti precursors, aqueous $TiCl_4$ can be converted into crystalline TiO_2 anatase at low temperature (80 °C, P_{atm}), as demonstrated in previous work [25]. Another benefit associated with the use of this precursor resides in its aqueous nature, which makes it much less susceptible to self-ignition, an important factor to consider in the scale-up of operations. Finally, the dynamics of the method described in this work, where the sample is irradiated while in motion on a small conveyor belt system, should enable a straight forward transition towards continuous roll-to-roll manufacturing. It is anticipated that the solution process described in this work, once automated, is easily applicable to large devices built on TCO-glass and further transferable to roll-to-roll processable substrates such as metal coils.

This work compares structural properties of sprayed vs. solution processed blocking layers. Emphasis is given to the effect of process parameters, for instance the number of sprays, concentration of the $TiCl_4$ precursor and impact of solvent modifications. The technological steps involved in the development and optimization of our solution deposition method are thoroughly explained and supported by optical microscope observations and wetting angle measurements. The morphological and crystalline properties of high temperature sprayed *vs.* solution processed blocking layers are further characterized using extensive electron imaging (FEG-SEM) and X-ray diffraction analyses. Finally, standard non-optimized I^-/I^{3-}-based liquid DSC devices were fabricated to probe the performance of solution processed TiO_2 blocking layers in minimizing electron recombination. This photovoltaic system was selected because the effect of pin-holes is much easier to observe when a substrate is put in contact with small ions in solution and has already been very well characterized in previous work [6-8]. Photovoltage decay measurements and I/V data were collected from devices built on solution processed and optimized sprayed TiO_2 blocking layers and electron lifetime plots were produced to compare the effectiveness of the different types of blocking layers.

Experimental

1) Preparation and characterization of solution processed blocking layers

Spray pyrolysis

A solution of 0.2 M titanium di-isopropoxide bis(acetylacetonate) (or TAA) in ethanol was manually sprayed with an art spray gun (Sealey, Model No. AB932) over the conductive surface of a fluorine-doped tin oxide (FTO)-coated glass, according to the method developed by Kavan et al. [1]. The substrate was pre-heated and maintained at 450 °C on a hotplate. A series of 1 to 50 sprays were applied successively at 10s intervals. One edge of the substrates was masked using a thin glass slide in order to create a clean step at the edge of the blocking layer, used to measure the thickness of material deposited.

Spin coating

A 240 mM solution of Ti tretraisopropoxide (99.99%, Sigma Aldrich) was prepared in ethanol with additional 7 µL/ml of 2 M HCl and filtered using 0.45 µm pore size filters. A total volume of 200 µL was dispensed over a 7.84 cm^2 TCO-coated glass substrate. Spin coating was carried out using 1 cycle at 500 rpm for 10s, immediately followed by a second cycle at 2000 rpm for 60s. The wet film was dried in an oven at 150 °C for 10 mins and sintered on a pre-heated hotplate at 450 °C for 30mins.

Solution processing

The precursor solution was prepared by dissolving titanium(IV) chloride tetrahydrofurane complex ($TiCl_4$·THF, ≥97.0 purum from Sigma Aldrich) in distilled water at a concentration of 10-30 g/L. Alternately, a mixed solvent of isopropanol (IPA) and distilled water at 30/70 v/v was employed, the addition of isopropanol aiming to improve the wetting properties of the precursor on the FTO-coated substrate. The precursor solution was spread across the surface of the substrate by doctor blading, at T_{amb}. The coated substrate was immediately transferred to the sample platform of the NIR oven and heat treated consecutively at 30 % and 80 % radiation power, over a total duration of 25s. The NIR equipment used in this work (Adphos NIR/IR Coil lab LV2) was described in detail in previous work [21]. The wetting properties of the precursor solution were investigated using an FTA 1000 B Class (First Ten Angstrom, USA) dynamic contact angle measurements apparatus. The data were computed from a series of snap shots of a single droplet released from the tip of a syringe onto the surface of a TEC 15 substrate using a high speed camera (up to 250 frames/s). Evolution of the shape of the droplet was recorded from its formation at the tip of the syringe to the point of contact with the substrate, release and equilibrium.

2) Characterisation

The structural properties of all types of blocking layers were extensively characterized using secondary electron microscopy (Hitachi S-4800, 12 keV, 10 µA, ~ 5 mm working distance). In the case of sprayed and solution processed layers, the crystalline properties were determined by glancing angle X-ray diffraction (XRD) measurements on a Panalytical X'pert Pro diffractometer (Cu K_α radiation λ = 1.5406 Å, 40 kV, 30 mA, and a 2θ range 10 - 70°, glancing angle of 1°). Thickness measurements were performed using a Dektak 150 profilometer equipped with a white light source optical microscope.

3) Fabrication of dye-sensitized solar cell devices

To probe the effectiveness of the different blocking layers dye cells with an active area of 1 cm^2 were prepared. The cells were not optimized for high efficiency. No $TiCl_4$ post treatment of the mesostructured titania layer was carried out and no extra scattering layer was added on top of the mesostructured titania. Working electrodes were fabricated on TEC15 (15 Ω/□, NSG) fluorine-doped tin oxide glass substrates covered with a blocking layer prepared by solution processing or spray deposited, and on bare TEC 15 glass substrates. A thin coating of TiO_2 paste (18 NR-AO from Dyesol, Australia) was bar coated and sintered at 450 °C for 30 mins. The thickness of the resulting films, 9.6 µm in average, was determined by stylus profilometry. The films were immersed overnight in a dye solution prepared by dilution of cis-bis(isothiocyanato)bis(2,20-bipyridyl-4,40-dicarboxylato)-ruthenium(II) bis-tetrabutyl-ammonium (N719, Dyesol) in acetonitrile: tert-butanol (50/50 v/v), assisted with ultrasonic agitation at T_{amb} for 1 hr. The films were further rinsed with ethanol and dried in air. Counter electrodes were prepared on pre-cut 1.5 x 2.5 cm^2 pieces of TEC 15. A 5 mM solution of chloro-platinic acid (H_2PtCl_6, Sigma Aldrich) in isopropanol was spread on the conductive side of the glass substrates and held in a pre-heated oven at 385 °C for 30min. Laser cut 25 µm thick Surlyn gaskets (Solaronix) were used as spacers. A standard I^-/I_3^- based electrolyte (0.8 M 1-propyl-3 methylimidazolium iodide (PMII), 0.3 M benzimidazole, 0.1 M I_2 and 0.05 M guanidinum thiocyanate dissolved in 3-methoxypropionitrile, all components from Sigma Aldrich) was vacuum filled through a 0.5mm hole pre-drilled in the counter electrode. Silver conductive paint was applied along the edges of the electrodes for optimization of current collection.

Open circuit photovoltage decay measurements were performed on the assembled cells to characterize the electronic properties of the different types of blocking layers. The cells were illuminated using a white LED light source (1 sun equivalent output) until the cells reached a steady state (for approximately 10 s), at which point illumination was interrupted. The photovoltage data were recorded over 60s using a Gamry Instrument Reference 600 potentiostat at a rate of 200 points/s. Decay data on a logarithmic time scale was smoothed using Loess smoothing to give evenly spaced data. The lifetime was then calculated using the reciprocal time-derivative of the voltage decay normalized to the thermal voltage [26]:

$$\tau_n = -\frac{k_B T}{q}\left(\frac{dV_{oc}}{dt}\right)^{-1}$$

Results and discussion

1) Structural properties of sprayed and spin-coated blocking layers

The fabrication of TiO_2 blocking layers by spray pyrolysis in application to liquid and solid-state DSCs has been reported by a number of research teams [1,2,4,5,17]. These studies suggest that the structural properties of sprayed TiO_2 compact layers vary significantly depending on the experimental set-up. For instance, parameters such as the distance of the spray gun nozzle to the substrate, the nature of the Ti-organo precursor, the nozzle design, the rheological properties and flow of the solvent, and particularly the use of automated vs. manual equipment, heavily impact upon the properties of the resulting TiO_2 compact layer. Despite such technical variability, spray pyrolysis remains the most reliable way to deposit high coverage yield (pin hole-free) TiO_2 compact layers on TCO-coated glass substrates at the laboratory scale. With this mind, we chose this method to produce a series of reliable control samples. The basic structural properties of these samples were compared to spin coated and solution processed layers.

TCO-glass substrates were coated with TiO_2 compact layers sprayed by application of 0, 1, 5, 15, 25 or 50 sprays. The data presented in Figure 1a show the average thickness values extracted from profilometry measurements, except for the case of a single spray where the thickness of material deposited was beyond instrumental resolution. These data show that the compact layers produced by spray pyrolysis increase in thickness from 7 to 35 nm with the application of 5 to 50 sprays, following a quasi linear progression. This trend is related to the multi-cycle aspect of the spray technique: the sequential deposition of very small equivalent amounts of material allows the linear buildup of a conformal compact layer. Figure 1b presents a cross sectional view of a TiO_2 layer deposited on a TCO-glass substrate by application of 50 sprays: the uniform thickness of the layer which follows the topology imposed by surface FTO crystals further illustrates the conformal nature of the deposition. Although not reported here, it was observed that for a much larger number of sprays the conformal character of the compact layer is progressively lost as the thickness supersedes the roughness of the substrate. This sample, when held under a white source of light had a uniform pale brown colour owing to birefringence effects.

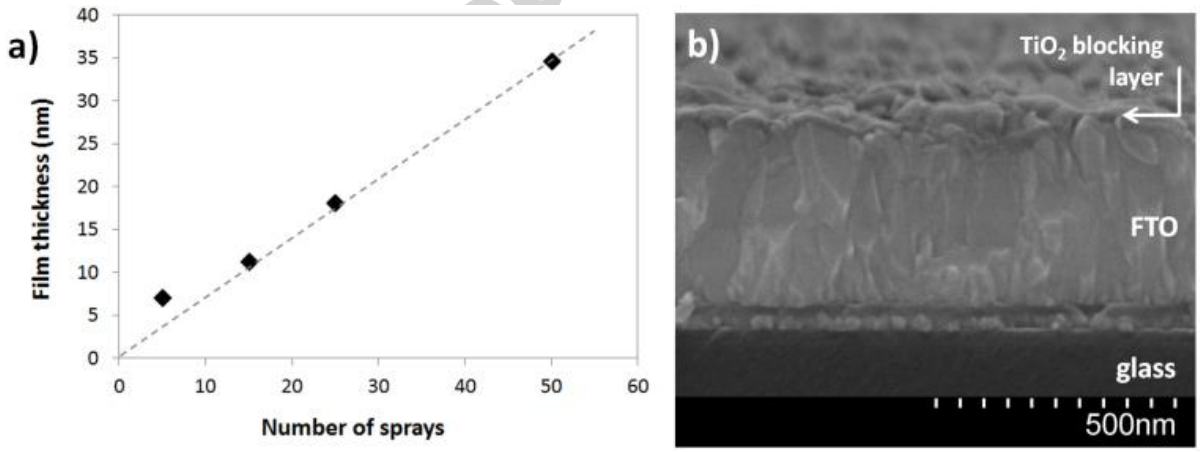

Fig. 1 Thickness of compact layers produced by application of 5-50 sprays (a). FEG-SEM cross sectional view of a TiO_2 compact layer deposited by spray pyrolysis (50 sprays) on a TCO-glass substrate (b).

Structural properties of sprayed compact layers were further characterized using top view electron microscopy, as shown in Figure 2a. At low magnification, all sprayed samples had a uniform surface apparently free of sub-micron size pin holes or impurities such as residual solvent or dust particles. High magnification images provided a better view over the progressive build-up of the

compact layer: with a single spray, the majority of the surface of the TCO-glass remained pristine and only few FTO crystals appeared to be covered with a thin skin of material; the application of 5 sprays and over was found to provide complete coverage of the substrate. The layer of material deposited using up to 5 sprays was visibly conformal to the FTO crystals, however, for 15 sprays and over, a change in roughness was observed related to the formation of small nodules in the valleys and peaks formed by the FTO crystals.

The compact layer obtained by spin coating was found to be populated with a high density of defects. In some areas, the fluctuation in thickness of material deposited was responsible for the formation of large pin holes, an excess of material causing the formation of cracks (insert 1) while too little exposed the surface of FTO crystals (insert 2), as illustrated in Figure 2b.

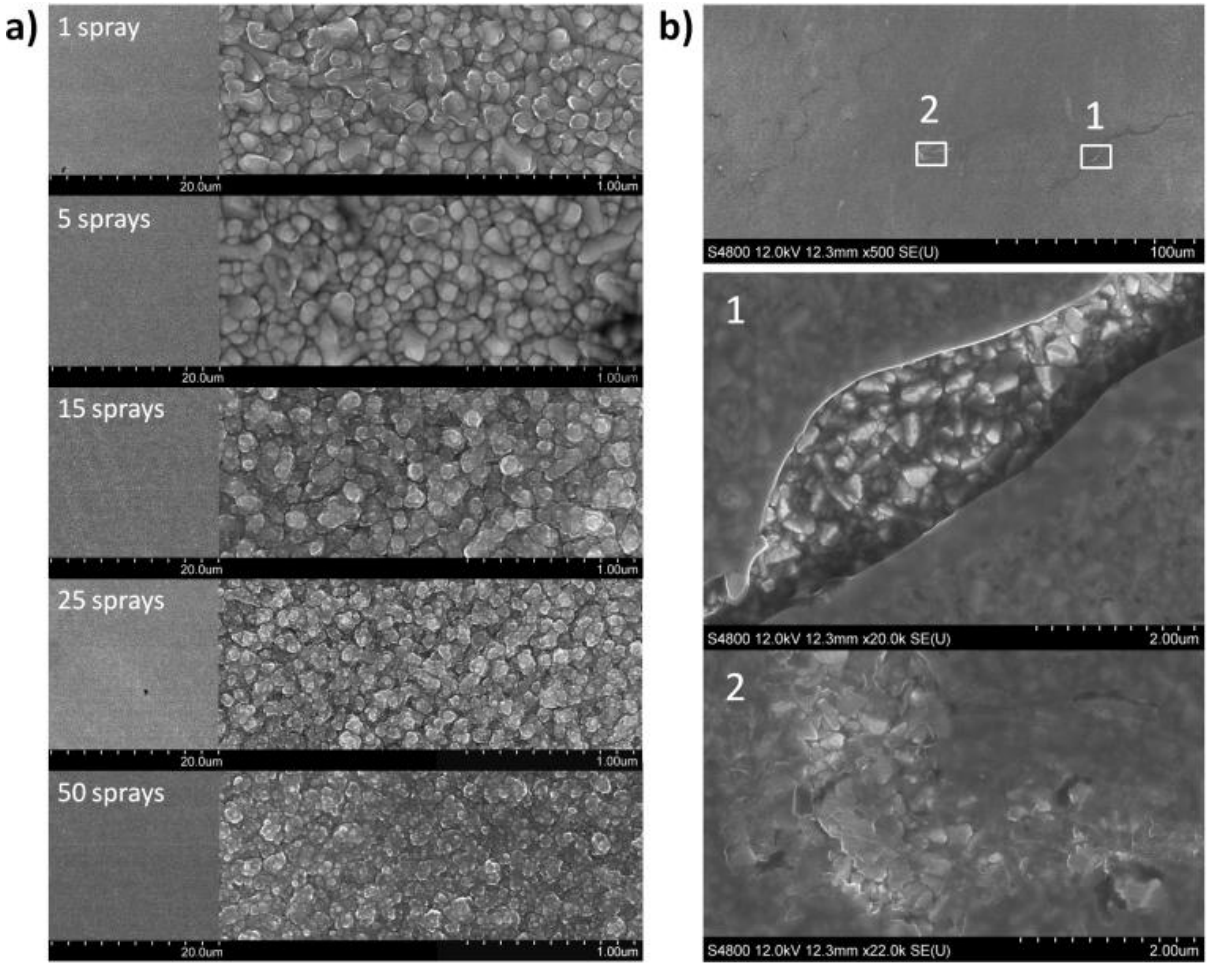

Fig. 2 Low (left) and high (right) magnification secondary electron images of compact layers prepared by spray pyrolysis (1 to 50 sprays) (a); Low magnification (top) of a compact layer prepared by spin coating (b) and high magnification of associated defects (inserts 1,2).

2) Deposition and characterization of solution processed blocking layers

a) Structural observations and colour-based thickness mapping

Developments related to solution processing of TiO_2 compact layers were inspired by previous work on the synthesis of crystalline TiO_2 nanoparticles obtained by controlled hydrolysis (P_{atm}, 80 °C) of a $TiCl_4$ aqueous precursor [25,27]. These studies showed that the kinetics of the hydrolysis reaction and properties of the resulting TiO_2 products could be controlled by adjusting the initial

concentration of the precursor; most importantly, it was possible to achieve the crystallization of dispersed 3-6 nm TiO_2 anatase nano-crystals in under 30 mins using a scalable batch inorganic process. Other work reports on the application of a $TiCl_4$ aqueous treatment aimed to improve the structural and anodic properties of mesoporous TiO_2 films in DSC devices [28,29]. In these studies, it is suggested that the nucleation of very small (approx. 1 nm) anatase crystals onto the pre-existing TiO_2 scaffold impacts on the electron recombination and electric field at the surface of the mesoporous titania. Based on the latter, $TiCl_4$·THF, a more stable version of $TiCl_4$ in water, was chosen as a Ti-based precursor for our take on solution processing of thin TiO_2 layers.

Basic physical and mechanical properties of TiO_2 layers obtained by hydrolysis of a 10 g/L $TiCl_4$·THF water-based precursor were first assessed on a film intentionally produced with variable thickness. A drop of the precursor solution was made to precipitate between two microscope slides maintained at an acute angle on a pre-heated hotplate at 80 °C, as illustrated in Figure 3a (insert). With this set-up the front of liquid precursor started to precipitate at the open side of the slides and water evaporation followed a lateral motion, providing the resulting film with a gradually increasing thickness. The film was found to be populated with cracks of increasing density and width from the thinner (left) to the thicker (right) side of the film. The thickness variation of the film was also evidenced by the appearance of coloured vertical stripes under white light illumination, as shown in Figure 3a. This coloured pattern is produced by refraction of white light through the variable thickness of the TiO_2 film, in the same way a thin film of oil spilled over water creates a coloured pattern in day light.

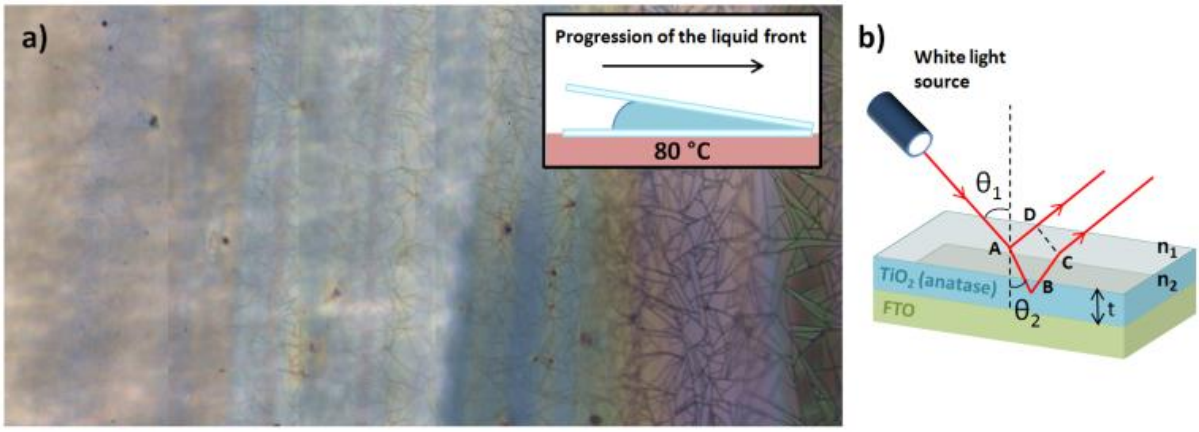

Fig. 3 Optical microscope image of a compact TiO_2 layer of increasing thickness (from left to right) prepared by solution processing of a 10 g/L $TiCl_4$·THF aqueous precursor (a); Optical path of a white light source at the interface air/thin film/FTO of the sample (b).

The schematic drawing illustrated as Figure 3b shows the optical path of a white light beam at the surface of this sample (θ_1 = 45°, $n_{1,air}$ = 1 and $n_{2,TiO2\ anatase}$). According to Fresnel's Law (Equation 1) the optical path difference (OPD) between the reflected and refracted beams is expressed as formulated in Equation 2.

$$n_1.\sin(\theta_1) = n_2.\sin(\theta_2) \quad \text{Eq. 1}$$

$$OPD = n_1.\overline{AD} - n_2.(\overline{AB} + \overline{BC}) = 2.n_2.t.\cos(\theta_2) \quad \text{Eq. 2}$$

Hence, the colours visible at the surface of the film under white light illumination arise from the mix of constructive and destructive interferences caused by the infinite number of monochromatic waves covering the visible range of light. This coloured pattern has been decomposed into a chart

named after its first inventor, Michel Levy [30], which associates each colour perceived by the human eye to a "m.λ" value. This chart has been used in a vast number of mineralogical publications for instance to determine the thickness of minerals directly observed under white light microscopy or to measure the birefringence characteristics of minerals under polarized light [31]. By correlating the colours visible at the surface of our solution processed blocking layers to the m.λ-indexed colours represented on the Michel Levy chart, and by application of Equation 3, an approximate thickness of the blocking layer was calculated.

$$m.\lambda = OPD = 2.n_2.t.\cos(\theta_2) \qquad \text{Eq. 3}$$

Table 1 provides the m.λ values extracted from Michel Levy's birefringence chart [30] in relation to the colours of the film shown in Figure 3a and the index of refraction of crystalline anatase (which varies accordingly to the wavelength of the incident light source [32]) and the corresponding thickness values calculated using Equation 3. Assuming the compact film is fully crystallized in the anatase TiO_2 phase, the data suggest that the compact film has a variable thickness ranging from 84 to > 210 nm (from left to right). The cracks observed to form in the light blue areas of the film suggest that the mechanical stability of the film is compromised above an approximate thickness of 120 nm. Contraction of the film upon drying is thought to be responsible for its mechanical instability. Moreover, the roughness of the FTO layer (~ 50 nm, according to Figure 2b) may contribute to additional stress by providing areas of higher and lower depth, in the valleys and at the top of the FTO crystals, respectively.

Table 1. Correlation between colour and film thickness of solution processed TiO_2 compact layers.

Colour of the film	m.λ (nm)	n_2	Thickness of the compact film (nm)
Light brown	400	2.80	74
Light purple	600	2.55	122
Blue-green	700	2.52	145
Yellow	800	2.50	167
Pink	1000	2.49	209

b) Wetting properties of the precursor

Improved control over the thickness of solution processed TiO_2 layers was carried out by modifying the wetting properties of the $TiCl_4$·THF precursor. Solvents with varied isopropanol/H_2O ratios were tested, up to 70/30 v/v water/isopropanol (IPA). Figure 4, shows dynamic contact angle measurements carried out on precursors prepared in 100 % H_2O or 70/30 v/v H_2O/IPA. These data demonstrate that with additional volumes of isopranol the contact angle of the precursor at t_0 (at the time when the drop is released from the syringe) decreases significantly from 42.1° to 20.7° by modifying the solvent composition from H_2O to 70/30 v/v H_2O/IPA. This difference keeps increasing as the droplet settles at the surface of the substrate until equilibrium where contact angle values stabilize at 9° for 70/30 v/v H_2O/IPA *vs*. 36° for the H_2O based precursor. Following these results, the mixed solvent precursor prepared in 70/30 v/v H_2O/IPA was selected to carry on with experimentation and further process optimization.

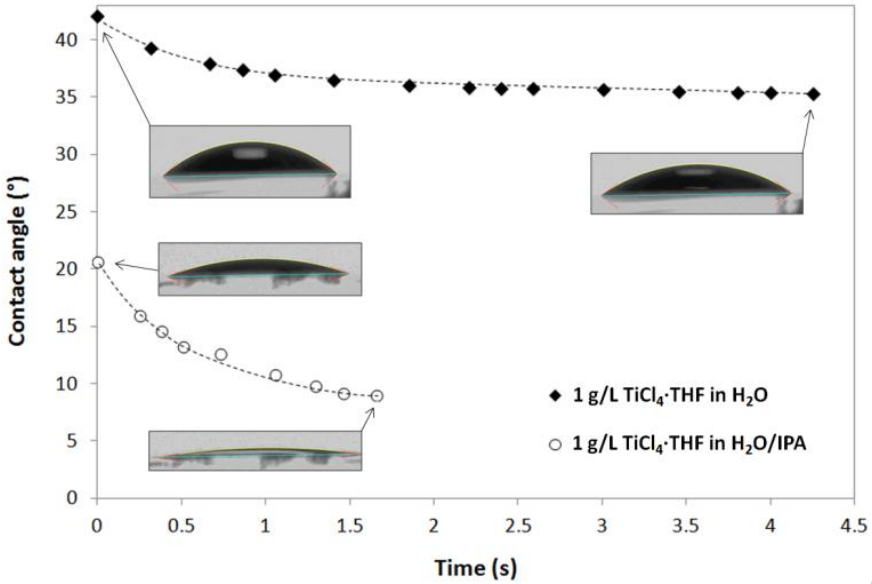

Fig. 4 Dynamic measurements of the wetting angle of 10 g/L $TiCl_4$·THF precursor prepared in H_2O and in H_2O/IPA (70/30 v/v) at the surface of TEC15 glass.

c) Film thickness and coverage

A series of films were produced by doctor blading a 10 g/L $TiCl_4$·THF-based precursor at T_{amb} through 100, 250 and 400 µm gaps (defining the spacing between the blade and the substrate), followed by application of a two-step NIR radiative treatment. Top view and cross section images of these films are presented Figure 5a-c. These demonstrate the non-conformal nature of the deposition with the deposited material filling the valleys formed by the FTO crystals. It also appears that the amount of material deposited increased with the size of the gap. The high and low magnification top views of these samples showed variable coverage levels: i) with a 100 µm gap, the amount of material deposited was not sufficient to fully cover all FTO surface and a high density of small pin holes and bare FTO crystal tops was visible; ii) with a 250 µm gap, most of the FTO surface was covered by the material deposited, however, the thickness of the deposit was thin enough to collect an imaged signal of the covered FTO layer and a number of pin holes were visible; iii) with a gap of 400 µm, the thickness of material deposited superseded the height of FTO crystals and was responsible for the generation of large cracks (typically 1-3 µm length) initiated upon contraction of the material during drying and sintering.

To avoid the formation of cracks and achieve a better coverage of the FTO layer, a double deposition at 100 µm gap was performed with an interval of 5 mins between the two depositions, allowing the substrate to cool down in between. The resulting film (Figure 5d) was found to provide a homogeneous coverage of the substrate with a very low density of pin holes compared to a single deposition. The few pin holes, only visible at high magnification, had a size < 50 nm. These observations suggested that a double deposition process provides compact layers with better inhibitive properties against electron recombination.

Because of the non-conformal nature of the material deposition associated to this process, the thickness of the compact films produced could not be measured using scanning profilometry. However, the coloured iridescence produced by the films (between light brown and purple) under white light and the observations made on cross sectional views of the NIR-stabilized deposits suggest that film thickness ranged between 30-50 nm, 50-100 nm and >100 nm for 100, 250, and 400 µm doctor blading gaps, respectively.

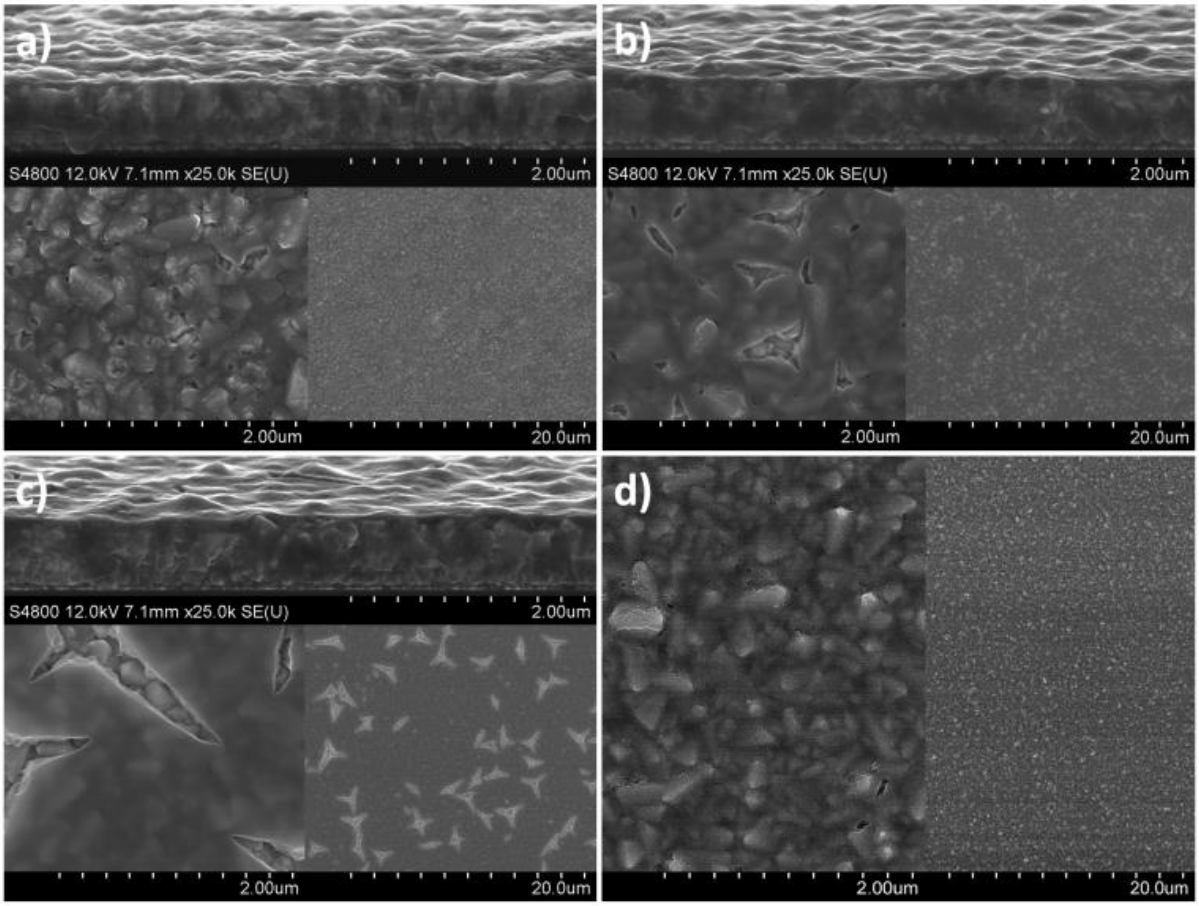

Fig. 5 Electron microscopy images (top views and cross sections) of solution processed blocking layers; substrate-to-blade gap: 100 µm -1 layer (a), 250 µm – 1 layer (b) and 400 µm – 1 layer (c); 100 µm – 2 layers (d).

d) Crystalline properties of NIR-processed layers

Finally, grazing angle x-ray diffraction analysis was performed on layers produced by spray pyrolysis and solution processed compact layers. The crystal size of the TiO_2 crystalline phase was estimated by application of the Scherrer equation to anatase (101) peak at 25.3°:

$$FWHM\ (2\theta) = \frac{K\lambda}{L.\cos(\theta)}$$

The full width at half maximum intensity was extracted from the Gaussian deconvolution of the anatase (101) peaks, as illustrated in the insert (Figure 6). The following assumptions were made: the peak broadening related to the instrument was considered negligible; the shape constant K = 0.9; the peak position θ = 25.3°, and the Cu K_α radiation λ = 1.5406 Å. These analyses confirm that both types of compact layers crystallized in the anatase phase of TiO_2. The crystalline range of layers produced by solution processing appeared to be smaller compared to sprayed layers, with an approximate average crystal size of 8 vs. 13 nm, respectively. It is thought that with spray pyrolysis, the slow and high temperature nature of the process allowed for the extension of the crystalline lattice according to the principle of Ostwald ripening. However, when using a short burst of NIR irradiative energy, the accelerated kinetics of the process favoured the nucleation over the growth of crystalline sites, hence leading to the formation of a TiO_2 anatase layer with a smaller average crystal range.

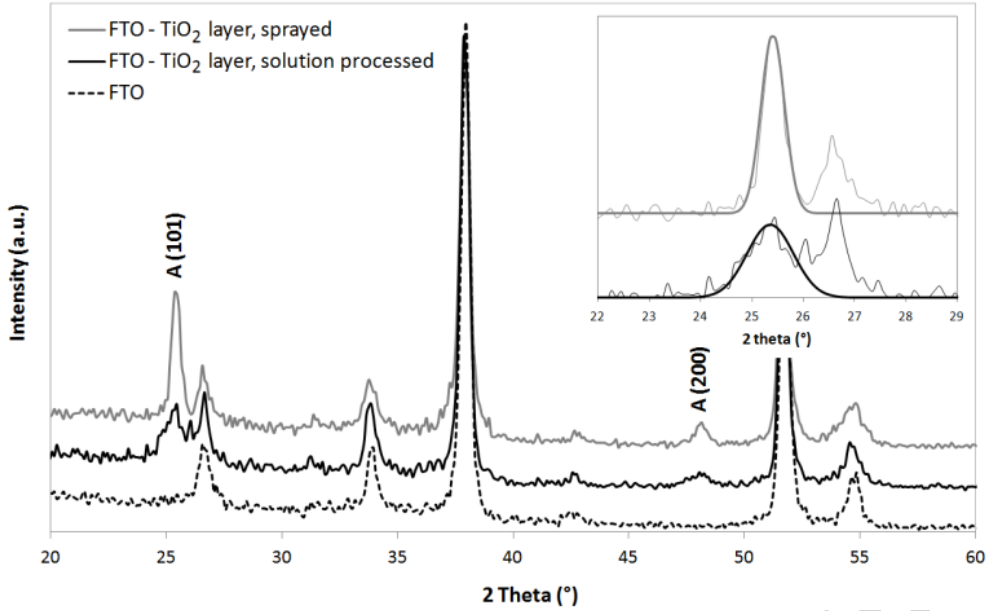

Fig. 6 Grazing incidence XRD measurements of sprayed (50 sprays) and solution processed blocking layers (2 layers of $TiCl_4$·THF in H_2O/IPA (70/30 v/v), 80 % NIR.

3) Performance of sprayed vs. solution processed blocking layers

In liquid electrolyte-based DSC devices, several contributions to electron back reaction have been identified: at the TiO_2 nanoparticles|electrolyte interface either via the conduction band or the trap states, and at the FTO|electrolyte interface. In their work on the function of blocking layers in liquid iodide/triiodide electrolyte-based DSCs, Cameron *et al.* demonstrated that at open circuit and low light conditions, the predominant recombination path for electrons is located at the FTO substrate|electrolyte interface [6-8]. The properties of the TiO_2 compact layer to minimize this phenomenon can easily be assessed by carrying out open circuit photovoltage decay measurements. Typically, when there is little recombination at the FTO substrate, e.g. the compact layer acts as an ideal electron recombination blocking layer, the rate of photovoltage decay slows down rapidly, reaching a quasi plateau at ~300 mV over 1min after dark. If the compact layer is not ideal, for instance due to the presence of pin holes, the photovoltage is expected to decay down to 0 V within a few seconds only.

Open circuit voltage decay data and associated lifetime plots collected from cells prepared with solution processed compact layers, no compact layer (control cell) and an optimized sprayed layer produced by spray pyrolysis (25 sprays) are presented in Figure 7. All cells were prepared with the same materials and fabrication process (except for the blocking layer) and had similar performance with power conversion efficiencies of ~ 3.3-4.8 % (the variability of which was assigned to the quality of the dye material, as well as film thickness and photoanode area of approx. 1 cm^2 considerations). The electron lifetimes are presented as a function of voltage rather than charge density. It is strictly correct to compare electron lifetimes measured at the same electron density; however as these cells were identical except for the blocking layers, the density of acceptor states should be broadly similar as a function of voltage allowing qualitative comparisons to be made between the cells.

In all cases the photovoltage was observed to decay rapidly after the light was switched off (at 5s, Figure 7a and 7b) but the rate of decay decelerated at longer times. In the case of an optimized blocking layer, the photovoltage was found to plateau towards 0.3 V, as expected from

previous work. The control cell, built on a bare substrate, showed the fastest decay down to 0 V after only 40s. The open circuit voltage (V_{oc}) was observed to increase from 662 mV for the control cell to 714 mV when using an optimized 25 spray blocking layer, a result of the minimization of the dark current. The lifetime plots produced from the photovoltage decays (Figure 7c and 7d) showed an improvement of the electron lifetime in the cell containing the optimized blocking layer. The electron lifetime was about six times longer at 0.6 V when compared to the cell without a blocking layer. The difference at longer times was more pronounced, when the photovoltage had decayed to 0.275 V, τ_n was 62s in the presence of an optimized blocking layer and 0.34s in the cell with no blocking layer.

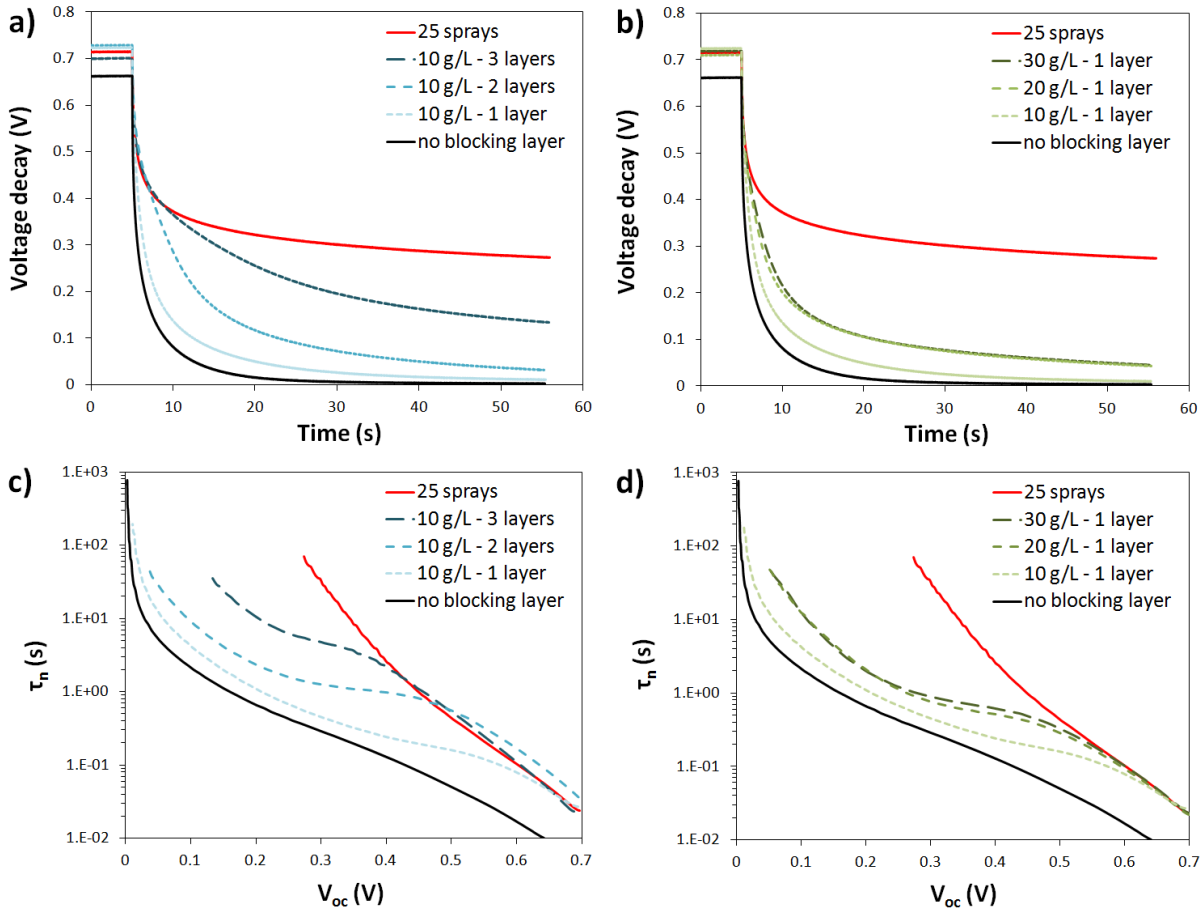

Fig. 7 Open circuit photovoltage decay measurements (a,b) and lifetime plots (c,d) of DSC devices prepared on solution processed blocking layers, no blocking layer and a 25 spray optimized blocking layer.

In the case of solution processed compact layers, the number of depositions was varied from 1 to 3 layers and the concentration of the precursor from 10 to 30 g/L $TiCl_4$·THF. Corresponding photovoltage decay and lifetime plots are presented in Figure 7 a,b and Figure 7 c,d, respectively. Compared to the control cell, it was found that the application of a single solution processed layer was effective in slowing the photovoltage decay, although at longer times the electron lifetime was similar to that in the cell without blocking layer. This is due to residual pin holes caused by a lack of material in small areas such as observed in Figure 5a (bottom left). Blocking behaviour was greatly improved by application of a 2nd or a 3rd consecutive layer, leading to a 4x and 16x increase in electron lifetime at 0.275 V, respectively. These results correlate with the electron microscope observations where the application of a second or more layers at a low precursor concentration (10 g/L) was found to reduce considerably the density of pin holes (Figure 5d), hence minimizing the

effect of electron recombination at the interface FTO|electrolyte. However, an increase in the concentration of the precursor solution had much less impact on the photovoltage decay. Cells containing blocking layers prepared with precursor concentrations of 20 g/L and 30 g/L showed the same OCVD decay characteristics, hence, there is a critical precursor concentration above which the single deposition of TiO_2 material no longer contributes to minimizing electron recombination. It is possible that an excessive thickness of material deposited as a single layer caused the formation of cracks, such as observed in the case of depositions using wide doctor blade gaps (Figure 5c). These defects provided large pathways allowing the electrolyte to contact the FTO substrate. Overall, this study demonstrates that the effectiveness of a TiO_2 blocking layer critically depends on structural properties, the coverage yield having a greater impact than the thickness.

Conclusions

In this work, we presented a fast and scalable approach for the deposition of a thin compact TiO_2 layer where a wet film of an inorganic titanium precursor ($TiCl_4$·THF) was doctor bladed across the surface of an FTO-coated glass substrate and rapidly hydrolyzed into a compact layer of crystalline TiO_2 using NIR radiation. The properties of this layer were assessed based on coverage yield, thickness, crystallinity and compared to compact layers obtained by conventional spray pyrolysis and spin-coating methods. It was shown that the sequential solution processing of 2-3 layers (in under 1min of processing time) based on our method provided compact layer with increasing coverage yield and very low pin holes density. In terms of coverage yield, thickness uniformity, and pin holes density, electron microscopy investigations showed the properties of solution processed TiO_2 blocking layers to be far superior compared to spin-coated ones where a high density of sub-micron size pin holes were caused by thickness irregularities.

When applied to the fabrication of I^-/I_3^- liquid based dye-sensitized solar cells, the sequential deposition of 3 solution processed layers reduced recombination substantially and even at 0.275 V the electron lifetime was nearly sixteen times longer when compared to a cell with no blocking layer. The difference in electron lifetimes between solution processed and spray pyrolysis at the longest times/lowest photovoltages are likely to be due to a small number of pinholes in the solution processed layers. Previous work [6] has shown that recombination via the FTO substrate dominates at longer times and lower photovoltages and that the rate of decay is strongly influenced by any pinholes in the blocking layer. Further optimization will be necessary for solution processing to achieve comparable coverage yield compared to spray pyrolysis in DSC. However, this result is extremely encouraging considering the overall process improvements introduced with our fabrication method (< 1min, roll-to-roll compatible) compared to the conventional spray pyrolysis method. Moreover, the small number of pinholes present is unlikely to be a problem in perovskite solar cells. Based on our recent research, it appears that in the case of lead halide perovskite solar cells, compared to ss-DSCs or cobalt based liquid DSCs, device output is significantly less affected by the presence of pin holes in the TiO_2 compact layer. Hence, solution processing of inorganic precursors such as demonstrated in this work may provide a very suitable and scalable alternative to the more recently adopted spin coating and atomic layer deposition methods which are not well suited for large scale applications. Future investigations will consider low-temperature solution processing of solution processed TiO_2 nanoparticle aqueous colloids in application to the fabrication of lead halide perovskite photovoltaics.

Acknowledgements

This work was funded by the Sêr Cymru Solar project, an initiative from the Welsh Government and the SuperSolar flexible grant funding EP/5017361/1.

References

[1] L. Kavan, M. Grätzel, "Highly efficient semiconducting TiO_2 photoelectrodes prepared by aerosol pyrolysis", *Electrochimica Acta*, **40**, 643-652, 1995.

[2] U. Bach, D. Lupo, P. Comte, J. E. Moser, F.Weissörtel, J. Salbeck, H. Spreitzer, M. Grätzel, "Solid-state dye-sensitized mesoporous TiO_2 solar cells with high photon-to-electron conversion efficiencies", *Nature,* 1998, **395**, 583.

[3] F. Fabregat-Santiago, J. Bisquert, L. Cevey, P. Chen, M Wang, S. M. Zakeeruddin, and M. Gratzel, "Electron Transport and Recombination in Solid-State Dye Solar Cell with Spiro-OMeTAD as Hole Conductor", *J. Am. Chem. Soc.* 2009, **131**, 558.

[4] B. Peng, G. Jungmann, C. Jäger, D. Haarer, H.-W. Schmidt, M. Thelakkat, "Systematic investigation of the role of compact TiO_2 layer in solid state dye-sensitized TiO_2 solar cells", *Coordination Chemistry Reviews*, 2004, **248** (13-14), 1479.

[5] F. Matteocci, G. Mincuzzi, F. Giordano, A. Capasso, E. Artuso, C. Barolo, G. Viscardi, T. M. Brown, A. Reale, A. Di Carlo, "Blocking layer optimisation of poly (3-hexylthiopene) based solid state dye sensitized solar cells", *Organic Electronics*, 2013, **14**(7), 1882.

[6] P. J. Cameron, L. M. Peter, "Characterization of Titanium Dioxide Blocking Layers in Dye-Sensitized Nanocrystalline Solar Cells", *J. Phys. Chem. B*, 2003, **107**, 14394.

[7] P. J. Cameron, L. M. Peter, "How Does Back-Reaction at the Conducting Glass Substrate Influence the Dynamic Photovoltage Response of Nanocrystalline Dye-Sensitized Solar Cells?", *J. Phys. Chem. B*, 2005, **109**, 7392.

[8] M. Bailes, P. J. Cameron, K. Lobato, L. M. Peter, "Determination of the Density and Energetic Distribution of Electron Traps in Dye-Sensitized Nanocrystalline Solar Cells", *J. Phys. Chem. B*, 2005, **109**, 15429.

[9] S. Hore, R. Kern, "Implication of device functioning due to back reaction of electrons via the conducting glass substrate in dye sensitized solar cells", *Appl. Phys. Lett.*, 2005, **87**, 263504.

[10] S. Ito, P. Liska, P. Comte, R. L. Charvet, P. Pechy, U. Bach, L. Schmidt-Mende, S. M. Zakeeruddin, A. Kay, M. K. Nazeeruddin, M. Grätzel, "Control of dark current in photoelectrochemical ($TiO_2/I^-–I_3^-$) and dye-sensitized solar cells", *Chem. Comm.*, 2005, 4351.

[11] S. M. Waita, B. O. Aduda, J. M. Mwabora, G. A. Niklasson, C. G. Granqvist, G. Boschloo, "Electrochemical characterization of TiO_2 blocking layers prepared by reactive DC magnetron sputtering", *Journal of Electroanalytical Chemistry,* 2009, **637**(1-2), 79.

[12] G. E. Eperon, V. M. Burlakov, P. Docampo, A. Gorielyand, H. J. Snaith, "Morphological Control for High Performance, Solution-Processed Planar Heterojunction Perovskite Solar Cells", *Advanced Functional Materials*, 2013, **24**(1), 151.

[13] A. K. Chandiran, A. Yella, M. T. Mayer, P. Gao, M. K. Nazeeruddin, and M. Grätzel, "Sub-nanometer conformal TiO_2 blocking layer for high efficiency solid-state perovskite absorber solar cells", *Adv. Mater.*, 2014, **26**, 4309.

[14] Q. Gao, S. Yang, L. Lei, S. Zhang, Q. Cao, J. Xie, J. Li, and Y. Liu, "An Effective TiO_2 Blocking Layer for Perovskite Solar Cells with Enhanced Performance", *Chem. Lett.*, 2015*,* **44**, 624.

[15] Y. Wu, X. Yang, H. Chen, K. Zhang, C. Qin, J. Liu, W. Peng, A. Islam, E. Bi, F. Ye, M. Yin, P. Zhang and L. Han, "Highly compact TiO_2 layer for efficient hole-blocking in perovskite solar cells", *Applied Physics Express*, 2014, **7**(5), 052301.

[16] J.-H. Yum, T. Moehl, J. Yoon, A. Kumar Chandiran, F. Kessler, P. Gratia, and M. Grätzel, "Toward Higher Photovoltage: Effect of Blocking Layer on Cobalt Bipyridine Pyrazole Complexes as Redox Shuttle for Dye-Sensitized Solar Cells", *J Phys. Chem. C*, 2014, **118**, 16799.

[17] W. Ke, G. Fang, J. Wan, H. Tao, Q. Liu, L. Xiong, P. Qin, J. Wang, H. Lei, G. Yang, M. Qin, X. Zhao and Y. Yan, "Efficient hole-blocking layer-free planar halide perovskite thin-film solar cells", *Nature Comm.*, 2015, **6**, 6700.

[18] C. Jiang, W. L. Koh, M. Y. Leung, W. Hong., Y. Li, J. Zhang, "Influences of alcoholic solvents on spray pyrolysis deposition of TiO_2 blocking layer films for solid-state dye-sensitized solar cells", *J. Solid State Chemistry*, 2013, **198**, 197.

[19] H.-S. Kim, C.-R.l Lee, J.-H. Im, K.-B. Lee, T. Moehl, A. Marchioro, S.-J. Moon, R. Humphry-Baker, J.-H. Yum, J. E. Moser, M. Gratzel, N.-G. Park, "Lead iodide perovskite sensitized all-solid-state submicron thin film mesoscopic solar cell with efficiency exceeding 9%", *Nature Scientific Reports,* 2012, **2**, 591.

[20] M. M. Lee, J. Teuscher, T. Miyasa, T. N. Murakami, H. J. Snaith, "Efficient hybrid solar cells based on meso-superstructured organometal halide perovskites", *Science*, 2012, **338** (6107), 643.

[21] T. Watson, I. Mabbett, H. Wang, L. Peter, and D. Worsley, "Ultrafast near infrared sintering of TiO_2 layers on metal substrates for dye-sensitized solar cells", *Progress in Photovoltaics: Research and Applications*, 2011, **19** (4), 482.

[22] M.J. Carnie, C. Charbonneau, P.R.F. Barnes, M.L. Davies, I. Mabett, T.M. Watson, B.C. O'Regan, D.A Worsley, "Ultra-fast sintered TiO_2 films in dye-sensitized solar cells: phase variation, electron transport and recombination", *Journal of Materials Chemistry A*, 2013, **1** (6), 2225.

[23] C. Charbonneau, K. Hooper, M. Carnie, J. Searle, B. Philip, D. Wragg, T. Watson and D. Worsley, "Rapid radiative platinisation for dye-sensitised solar cell counter electrodes", *Progress in Photovoltaics: Research and Applications*, 2014, **22**(12), 1267.

[24] M. Cherrington, T.C. Claypole, D. Deganello, I. Mabett, T. Watson, D. Worsley, "Ultrafast near-infrared sintering of a slot-die coated nano-silver conducting ink", *Journal of Materials Chemistry*, 2011, **21** (21), 7562.

[25] C. Charbonneau, R. Gauvin, G. P. Demopoulos, "Aqueous solution synthesis of crystalline anatase nanocolloids for the fabrication of DSC photoanodes", *J. Electrochem. Soc.*, 2011, **158** (3), H224.

[26] A. Zaban, M. Greenshtein and J. Bisquert, "Determination of the Electron Lifetime in Nanocrystalline Dye Solar Cells by Open-Circuit Voltage Decay Measurements", *ChemPhysChem*, 2003, **4**, 859.

[27] C. Charbonneau, R. Gauvin, G. P. Demopoulos, "Nucleation and growth of self-assembled nanofibre-structured rutile (TiO_2) particles via controlled forced hydrolysis of titanium tetrachloride solution", *J. Crystal Growth*, 2009, **312**(1), 86.

[28] P. M. Sommeling, B. C. O'Regan, R. R. Haswell, H. J. P. Smit, N. J. Bakker, J. J. T. Smits, J. M. Kroon, and J. A. M. van Roosmalen, "Influence of a $TiCl_4$ post-treatment on nanocrystalline TiO_2 films in dye-sensitized solar cells", *J. Phys. Chem. B*, 2006, **110**, 19191.

[29] B. C. O'Regan, J. R. Durrant, P. M. Sommeling, N. J. Bakker, "Influence of the $TiCl_4$ Treatment on Nanocrystalline TiO_2 Films in Dye-Sensitized Solar Cells. 2. Charge Density, Band Edge Shifts, and Quantification of Recombination Losses at Short Circuit", *J. Phys. Chem. C*, 2007, **111**, 14001.

[30] B. E. Sorensen, "A revised Michel-Lévy interference colour chart based on first-principles calculations", *Eur. J. Mineral.*, 2013, **25**, 5.

[31] http://www.werkstoff-in-der-praxis.de/anwendungen/kursprogramm/michel-levy-color-chart.pdf

[32] G. E. Jellison, L. A. Boatner, and J. D. Budai, "Spectroscopic ellipsometry of thin film and bulk anatase (TiO_2)", *J. Applied Phys.*, 2003, **93** (12), 9537.